Quantitative Structural Study of Cold-Crystallized PEKK

Sylvie Tence-Girault, Jonathan Quibel, Alexis Cherri, Sébastien Roland, Bruno Fayolle, Stéphane Bizet, Ilias Iliopoulos

▶ **To cite this version:**

Sylvie Tence-Girault, Jonathan Quibel, Alexis Cherri, Sébastien Roland, Bruno Fayolle, et al.. Quantitative Structural Study of Cold-Crystallized PEKK. ACS Applied Polymer Materials, 2021, 3 (4), pp.1795-1808. 10.1021/acsapm.0c01380 . hal-03268680

HAL Id: hal-03268680
https://hal.science/hal-03268680

Submitted on 23 Jun 2021

HAL is a multi-disciplinary open access archive for the deposit and dissemination of scientific research documents, whether they are published or not. The documents may come from teaching and research institutions in France or abroad, or from public or private research centers.

L'archive ouverte pluridisciplinaire **HAL**, est destinée au dépôt et à la diffusion de documents scientifiques de niveau recherche, publiés ou non, émanant des établissements d'enseignement et de recherche français ou étrangers, des laboratoires publics ou privés.

Quantitative Structural Study of Cold-Crystallized PEKK

Sylvie Tencé-Girault,* Jonathan Quibel, Alexis Cherri, Sébastien Roland, Bruno Fayolle, Stéphane Bizet, and Ilias Iliopoulos

ABSTRACT: Poly(ether ketone ketone) (PEKK) is a semicrystalline polymer investigated for highly demanding applications in aerospace, transportation, electronics, and oil & gas industries. The properties required for these applications, such as thermomechanical and chemical stability, are intimately linked to the crystalline state of the material. PEKK exhibits a polymorphism that depends, among other factors, on its thermal history. The control and quantification of the crystalline state of PEKK is the subject of this study. Amorphous PEKK (T/I = 60/40, where T stands for terephthalic and I for isophthalic units) films were cold-crystallized at various crystallization temperatures, T_C, from 180 to 280 °C in a ventilated oven. Based on a quantitative analysis of small-angle X-ray scattering (SAXS), wide-angle X-ray scattering (WAXS), and differential scanning calorimetry (DSC) data, we propose for the first time a methodology to obtain detailed information about the crystalline state of PEKK: total crystallinity, relative amount and stability of crystalline forms, form I and form II, and melting enthalpy of 100% crystallized PEKK. The evolutions of each crystalline form and the total crystallinity with T_C were deduced. The amount of each crystalline form, form I and form II, can be tuned by controlling the heating rate to 280 °C. The evolution of the crystalline lamellar thickness and periodicity as well as the crystalline amount and cell parameters with T_C were interpreted and discussed in relation to the published results on PEEK, PEKK (100% T), and PEKK (100% I). Finally, the melting enthalpy of a 100% crystallized PEKK copolymer (T/I = 60/40), $\Delta H_m^{100\%}$ = (202 ± 20) J/g, was estimated.

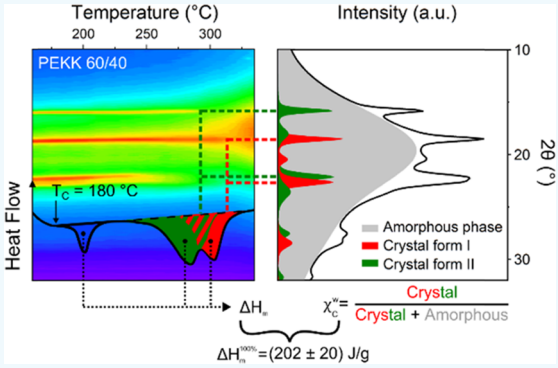

KEYWORDS: *poly(ether ketone ketone), crystallization, polymorphism, melting enthalpy, SAXS−WAXS*

1. INTRODUCTION

Semicrystalline polymers are increasingly used as structural materials in industrial sectors such as aerospace, automotive, and oil & gas industries. They exhibit outstanding physical properties due to their particular organization. They crystallize only partially and are composed of crystalline lamellae that alternate with the amorphous phase. Most of the macromolecular chains participate in both phases, being organized in the crystal lamellae and disordered and entangled in the amorphous phase. Macroscopic properties, such as mechanical, optical, ferroelectricity, thermal stability, or permeability, depend on the crystalline structure, the entanglement density of the amorphous phase, and the semicrystalline morphology.[1,2] The crystalline structure and morphology of semicrystalline polymers are defined by the chemical structure and flexibility of the macromolecular chains and also by the process used to prepare polymer parts.[3,4] Moreover, for polymers exhibiting relatively slow crystallization rates, the crystalline structure may evolve during post-process treatments or during use.[5]

It is mostly the crystalline structure that defines the macroscopic properties. Moreover, a number of semicrystalline polymers exhibit polymorphism.[6−9] For example, poly(vinylidene fluoride) (PVDF) can crystallize in five crystalline phases, characterized by different molecular conformations along the chain.[7] Among these crystalline structures, only one phase exhibits ferroelectric and piezoelectric properties.[7] The impact of polymorphism on mechanical properties has been particularly studied.[10,11] Numerous publications describe this influence in syndiotactic polystyrene,[8,12] syndiotactic polypropylene (s-PP),[10] various polyamides, such as PA6[13] or PA11,[14] or in poly(L-lactic acid) (PLLA).[15] Polymorphic transformations during stretching have also been reported in s-PP,[10] PVDF,[7] or PA11[14] and play a key role in mechanical behavior. Although the relationship between polymorphism and mechanical properties is particularly well documented, the crystalline structure can influence other macroscopic properties such as permeability.[15] For these semicrystalline polymers, the strong link established between the crystalline structure and macroscopic properties gave rise to numerous structural

Received: December 16, 2020
Accepted: February 25, 2021
Published: March 9, 2021

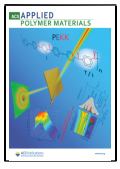

studies aimed at obtaining and quantifying these specific crystalline phases. This is particularly the case for PVDF[7] and s-PP.[10]

In this study, we are interested in poly(ether ketone ketone) (PEKK), a high-performance semicrystalline polymer showing polymorphism for which no clear relationship has been established with macroscopic properties. PEKK has outstanding high-temperature performance, high stiffness, tensile and compressive strength, and impacts resistance. PEKKs are prepared from diphenyl ether (DPE), terephthalic acid with *para*-phenyl links (*T* units), and isophthalic acid with *meta*-phenyl links (*I* units).[16] By varying the *T*/*I* ratio, the symmetry and the architecture of the aromatic macromolecule change, while the chemical composition remains the same. A variety of kinetics and crystallization states is associated with this adjustable *T*/*I* parameter.[17]

The crystallization of polymers of the poly(aryl ether ketones) (PAEK) family has been studied since the 1980s.[18−20] It is noteworthy that in PAEK, the glass transition and melting temperatures increase slowly and continuously with the ketone content, 33% ketone for poly(ether ether ketone) PEEK (T_g = 133 °C; T_m = 335 °C), 50% for PEK (T_g = 150 °C; T_m = 365 °C), 60% for PEKEKK (T_g = 153 °C; T_m = 370 °C), and 67% for PEKK (T_g = 160 °C; T_m = 385 °C).[21,22] For the ketone content higher than 50%, two crystalline phases, namely, form I and form II, appear depending, for instance, on whether the polymer is crystallized from the melt or the glassy state.[20] The details on the relative amount and stability of each form are still unknown. This polymorphism was first studied in PEKK in the years 1992−1996 by X-ray diffraction (wide-angle X-ray scattering, WAXS), thermal analysis (differential scanning calorimetry, DSC), and transmission electron microscopy (TEM).[17,22−24] More recently, with the development of the PEKK materials for use in additive manufacturing and thermoplastic composites, new studies have been published.[25−27] The authors focus on the influence of the *T*/*I* ratio on the kinetics of crystallization,[28] on the dynamical mechanical properties,[29] as well as on the influence of the thermal history on the mechanical properties.[30]

Most often, the two crystalline forms, form I and form II, coexist in PEKK and it is not clear how to promote one or the other or if thermal or mechanical transitions between these two forms exist. Nonetheless, these may be crucial pieces of information for applications. As an example, for laser sintering additive manufacturing, the crystallization state of the powder is a key parameter conditioning the process parameters.[31,32] To improve our knowledge in this field, the first essential step is to quantify the proportion of these two crystalline forms in PEKK, their melting temperature, and the global crystalline ratio. The first goal of this present study is to develop a quantitative method to analyze WAXS spectra. WAXS spectra analysis, based on the peak-fitting method, is detailed, compared with the absolute method published by Ruland in 1961;[33] its advantages and limitations are discussed.

Armed with this method, the second objective is to study the influence of cold-crystallization conditions (CC) on the structure and morphology of PEKK. PEKK films have been prepared with different amounts of crystalline form I and form II by cold crystallization at different temperatures and then studied by X-ray diffraction and thermal analysis. The peak-fitting method leads to a weight crystallinity (χ_c^w) close to the value deduced from the absolute method and in addition provides quantitative information on each crystalline form, the crystallinities (χ_{cI}^w and χ_{cII}^w), and the cell parameters. The analysis of the small-angle X-ray scattering (SAXS) spectra provided a measure of the crystalline lamellar thickness and periodicity for each crystallization temperature. Finally, *in situ* WAXS experiments along a thermal ramp, carried out at the Soleil synchrotron facility, allowed us to associate various melting endotherms with the specific crystalline forms (form I and form II). This new knowledge will be very useful to understand the impact of the crystallization state on applicative properties.

2. EXPERIMENTAL SECTION

2.1. Materials. The PEKK used in this study was provided by Arkema[34] as an amorphous 50 μm thick film (density at 23 °C = 1.27 g/cm^3).[35] It was obtained by cast extrusion of PEKK 6002 resin, which was prepared from diphenyl ether (DPE), terephthalic acid (*T*) with *para*-phenyl links, and isophthalic acid (*I*) with *meta*-phenyl links with a *T*/*I* ratio of 60/40 (Figure 1). PEKK 6002 has a weight-average molecular weight (M_w) of ca. 70 kg/mol.[28]

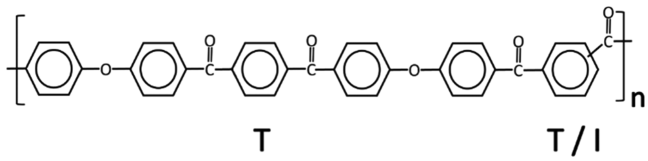

Figure 1. Chemical structure of PEKK copolymers with a random distribution of *T*−*T* and *T*−*I* units.

Among the commercially available grades of PEKK,[34] this *T*/*I* ratio is particularly interesting and widely used[29,25] because it crystallizes slowly.[22] Thus, depending on the process used, amorphous or semicrystalline material can be obtained. It is therefore essential to understand and manage how thermal treatment can induce the cold crystallization of the material.

Pieces of the PEKK 6002 film with a dimension of 5 × 10 cm^2 were put on Teflon sheets in perforated aluminum boxes in a ventilated oven preheated at the temperature of crystallization, T_C. After 24 h, the boxes were taken out of the oven and cooled down in an ambient atmosphere. T_C is fixed at 180, 200, 230, 250, and 280 °C. The estimated heating and cooling rates are around 15 °C/min. For comparison, an additional sample was prepared by melt crystallization; after 5 min in the melt at 360 °C, the sample was cooled (40 °C/min) and crystallized 4 h at 280 °C, in the DSC oven.

2.2. Differential Scanning Calorimetry (DSC). DSC measurements were performed using a Q1000 series TA Instruments. Disks of polymer films were cut using a cylindrical shape punch (diameter 3 or 6 mm) and stacked in a DSC aluminum pan to reach 7−10 mg. The first heating ramp was set at 10 °C/min under nitrogen flow (50 mL/min) from 20 to 350 °C unless otherwise stated.

2.3. Simultaneous SAXS−WAXS Experiments. Simultaneous SAXS−WAXS experiments were performed on the Nano-inXider SW (Xenocs, Sassenage, France) system in the transmission mode using Cu Kα radiation (λ = 1.54 Å) from an X-ray microsource (GeniX3D) operating at 50 kV−0.6 mA (30 W). Scattering patterns were collected using the combination of two detectors, Pilatus3 (Dectris), operating simultaneously in SAXS and WAXS positions. The entire system, from the source to the sample and to the two detectors, is under vacuum. Distances between the sample and the SAXS and WAXS detectors are fixed, allowing a continuous *q* range between 0.01 and 4.2 Å^{-1} (2θ range between 0.15 and 62°). The X-ray beam spot has a diameter of 800 μm. SAXS and WAXS patterns were recorded for 600 s. The corrected two-dimensional (2D) data were azimuthally integrated using Foxtrot data reduction software (version 3.4.9),[36] then normalized to the number of transmitted photons and to the sample thickness. After subtraction of a blank (spectra without

sample), the SAXS and WAXS profiles ($I_{Raw}(q)$, $I_{Raw}(s)$, or $I_{Raw}(2\theta)$) were treated to extract quantitative structural values. The scattering vectors q and s are defined as $q = 2\pi \times s = 4\pi\frac{\sin\theta}{\lambda}$, where 2θ is the Bragg angle.

WAXS spectra, $I_{Raw}(2\theta)$, were fitted using Fityk 0.9.8 software[37] in a wide 2θ range [5, 60°]. With this software, the WAXS spectrum was decomposed into crystalline and amorphous contributions. The crystalline peaks are associated with sharp peaks, located at the Bragg angle $2\theta_{hkl}$, while broad peaks fit the amorphous signal.

The interplanar distance d_{hkl} (distance between the (hkl) planes into the crystalline phase) was deduced from the Bragg angle $2\theta_{hkl}$ using the Bragg law

$$2d_{hkl}\cdot\sin\theta_{hkl} = \lambda$$

The weight crystallinity χ_c^w was calculated using the following equation

$$\chi_c^w = \frac{A_c}{A_t} \text{ with } A_t = A_c + A_a$$

A_c is the sum of the integrated intensities of the crystalline peaks, A_t is the total integrated intensity, and A_a is the total integrated intensity of the amorphous halo. A_c, A_t, and A_a are calculated in the required wide 2θ range from 5 to 60° (q from 0.36 to 4.1 Å^{-1}). The resulting weight crystallinity, calculated in this wide 2θ range will be compared to the absolute crystallinity calculated from the Ruland method.[33] Although this peak-fitting method for crystallinity calculation is widely reported,[38−41] it is not often used in this wide 2θ range.

To apply the absolute method, WAXS spectra, $I_{Raw}(s)$, were first corrected from absorption, polarization, and the Lorentz factor using XSACT software (Xenocs).[42] Then, the corrected WAXS spectra, $I_{corr}(s)$, were normalized to absolute units and the calculated incoherent intensity, $I_{incoh}(s)$, was subtracted. The used procedure is detailed in refs 43, 44. Intensities from crystalline peaks, $I_c(s)$, were extracted from the total coherent intensity, $I(s)$, without refinement treatment. The full procedure is reported in the Supporting Information.

In semicrystalline polymers, crystals grow to form crystalline lamellae. These lamellae are periodically organized, and the amorphous phase is intercalated between the crystalline lamellae. A correlation peak characterizing this periodic organization can be observed in SAXS spectra. The period of this organization, L_P, named the ≪long period≫, the ≪long spacing≫, or the ≪lamella spacing≫, is deduced from the position, q_{max}, of this correlation peak

$$L_P = \frac{2\pi}{q_{max}}$$

In this study, a more quantitative analysis of SAXS profiles was performed, the one-dimensional (1D) electron density correlation function, $K(z)$, along the lamellar normal direction z, was calculated. This calculation was integrated with XSACT software.[42] The crystalline lamellar thickness (L_c) and periodicity (L_P) can be derived from $K(z)$.[45] The detailed procedure used for this calculation was already published[46]

$$L_P = L_c + L_a$$

where L_a is the thickness of the amorphous phase in between two crystalline lamellae.

2.4. *In Situ* WAXS Experiments during Crystalline Phase Melting. *In situ* WAXS experiments were carried out on the high brilliance SWING beamline at the Soleil synchrotron facility (project no: 20170187). The beam energy was set at 17 keV, leading to a wavelength of 0.73 Å. Diffraction patterns were recorded using a CCD detector at 50 cm from the sample. The acquisition time was set to 1 s every 10 s. PEKK films (50 μm thick) were put in between two mica sheets (25 μm thick) in a Linkam THMS 600 heating plate controlled by a T96 controller and cooled by liquid nitrogen. The heating rate during *in situ* analyses was set to 10 °C/min. 1D WAXS pattern curves were obtained by circular averaging of the 2D images using Foxtrot software.

3. RESULTS

Simultaneous SAXS−WAXS experiments were performed on as-received PEKK 6002 films and after cold crystallization for 24 h at a temperature ranging from 180 to 280 °C. No significant orientation appears on 2D SAXS and WAXS images. Isotropic images were then azimuthally integrated to obtain SAXS and WAXS profiles.

The as-received film was amorphous, as no Bragg peaks were detected on the WAXS spectrum (Figure 2a) and no correlation peak appeared on the SAXS spectrum, as we will see in Section 3.3. After crystallization, SAXS and WAXS diffraction peaks appeared. Their position and intensity depend on the crystallization temperature.

3.1. Crystalline Phases and Crystallinity, WAXS Spectra. First, the quantitative analysis of WAXS spectra, based on a peak-fitting method using Fityk software[37] will be presented, and then these results will be compared with the method proposed by Ruland in 1961[33] for the calculation of the absolute crystallinity of polymers.

3.1.1. Quantitative Peak-Fitting Analysis of WAXS Spectra. In the WAXS spectra of Figure 2a, the Bragg peaks from the two crystalline forms, form I and form II, are observed. In Figure 2d, a pure form I film is reported, and this film was crystallized from the melt during 4 h at 280 °C. The proportion of each form depends on the crystallization temperature. The amount of form I, Φ_I, the total weight crystallinity, χ_c^w, and the weight crystallinity of form I and form II, χ_{cI}^w and χ_{cII}^w, were quantified using the following equations

$$\Phi_I = \frac{A_I}{A_I + A_{II}}, \chi_c^w = \frac{A_c}{A_t} = \frac{A_c}{A_c + A_a} = \chi_{cI}^w + \chi_{cII}^w$$

with

$$\chi_{cI}^w = \Phi_I \times \chi_c^w \text{ and } \chi_{cII}^w = (1 - \Phi_I) \times \chi_c^w$$

where A_I and A_{II} are the areas under the fitted crystalline peaks associated, respectively, with the crystalline form I and form II, $A_c = A_I + A_{II}$ and A_a is the integrated intensity of the amorphous halo.

The first step is to separate the intensity contributions arising from the crystalline and the amorphous regions and calculate A_I, A_{II}, and A_a. To do so, the WAXS spectra were decomposed using Fityk software,[37] with broad and sharp peaks, respectively, associated with the amorphous and crystalline phases. As the as-received sample is amorphous, its WAXS spectra were used to define the shape of the amorphous halo. Three broad pseudo-Voigt peaks were used to model this halo (Figure 2c). This amorphous halo characterizes PEKK amorphous samples, while for the semicrystalline films, some small deviations from this shape are allowed because small evolutions of the amorphous phase constrained between crystalline lamellae have been already observed.[47] Knowing the orthorhombic cell parameters of the form I and form II,[24] the interplanar distances, d_{hkl}^I and d_{hkl}^{II}, associated with each crystalline form can be calculated using the following expression (see Figure S1 in the Supporting information for a schematic of the crystal cells of form I and form II).

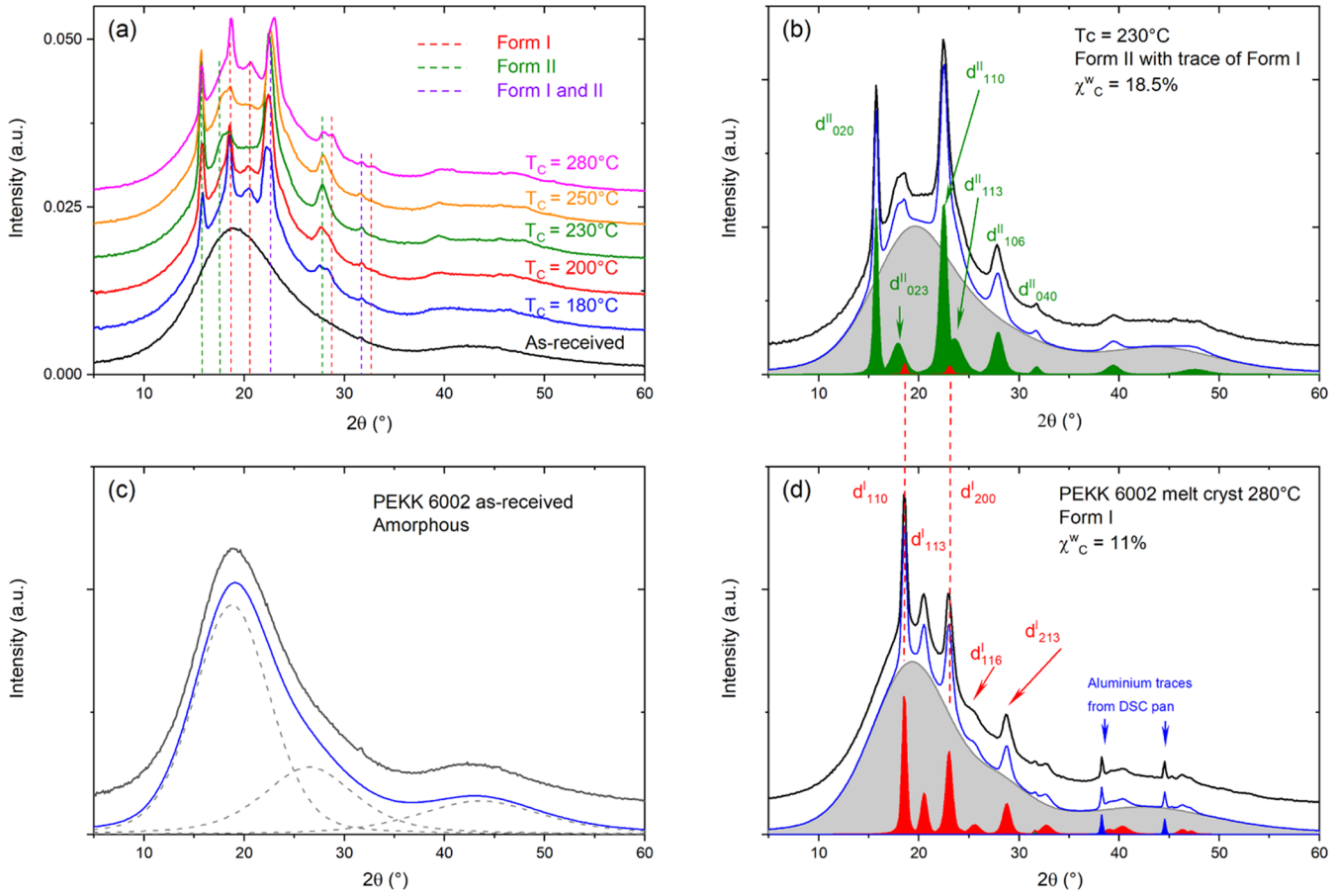

Figure 2. Evolution of the WAXS spectra for the different crystallization temperatures T_C. (a) Superposition of the spectra. (b) Decomposition of the WAXS spectra of form II (with traces of form I) in amorphous (gray) and crystalline peaks (green) for T_C = 230 °C. (c) As-received film with the decomposition of the amorphous signal in three broad peaks (dotted gray lines). (d) Decomposition of the WAXS spectra of form I in amorphous (gray) and crystalline peaks (red) for a sample melt-crystallized 4 h at 280 °C. In (b), (c), and (d), the blue lines correspond to the sum of the broad and sharp peaks obtained after the peak fitting, while the black lines correspond to the experimental spectra before the baseline subtraction.

$$d_{hkl} = \left[\left(\frac{h}{a}\right)^2 + \left(\frac{k}{b}\right)^2 + \left(\frac{l}{c}\right)^2\right]^{-1/2}$$

Then, each measured Bragg peak was attributed to a specific crystalline form I or form II. In Figure 2b,d, WAXS spectra indexation of pure form II and form I are shown. Form II with only small traces of form I was obtained after cold crystallization at 230 °C, while the pure form I was crystallized from the melt at 280 °C.

In some cases, the calculated interplanar distances of form I and form II are very close, for example, d^{I}_{200} of form I and d^{II}_{110} of form II (Table 1), and their corresponding calculated Bragg peaks are too close to be resolved, which leads to a single broad diffraction peak observed at $2\theta \sim 22.7°$. To obtain a reliable calculation of Φ_I, the existence of all of the calculated diffraction lines reported in Table 1 was imposed for the decomposition of the WAXS spectra and constraints for some adjustable parameters, such as widths and/or relative intensities, were applied for specific Bragg peaks. Only the Bragg peaks located at Bragg angles $2\theta < 30°$ (i.e., interplanar distances higher than 3 Å) are considered for the calculation of Φ_I. The detailed procedure used for peak fitting is reported in the Supporting Information.

Table 1. Calculated Interplanar Distances, d_{hkl}, and Bragg Angles, $2\theta_{hkl}$, for the Form I and Form II Using Published Cell Parameters[24] and Comparison to the Observed Bragg Angles

form I a = 7.78 Å, b = 6.10 Å, c = 31.13 Å			form II a = 4.17 Å, b = 11.08 Å, c = 31.13 Å			observed diffraction line
(hkl)	d^{I}_{hkl} (Å)	$2\theta^{I}_{hkl}$ (deg)	(hkl)	d^{II}_{hkl} (Å)	$2\theta^{II}_{hkl}$ (deg)	$2\theta_{obs}$ (deg)
			(020)	5.54	16.0	15.7
			(023)	4.89	18.15	17.9
(110)	4.80	18.48				18.5
(113)	4.36	20.38				20.5
(200)	3.89	22.86	(110)	3.90	22.79	22.5–23.0
			(113)	3.65	24.37	23.7
(116)	3.52	25.28				25.7
			(106)	3.25	27.44	27.9
(213)	3.13	28.54				28.8
			(040)	2.77	32.32	31.7

Results for the film crystallized at 180 °C are shown in Figure 3a. The evolutions of the total weight crystallinity, χ^w_c, and the crystallinity relative to form I and form II, χ^w_{cI} and χ^w_{cII}, with the crystallization temperature, are reported in Figure 3b.

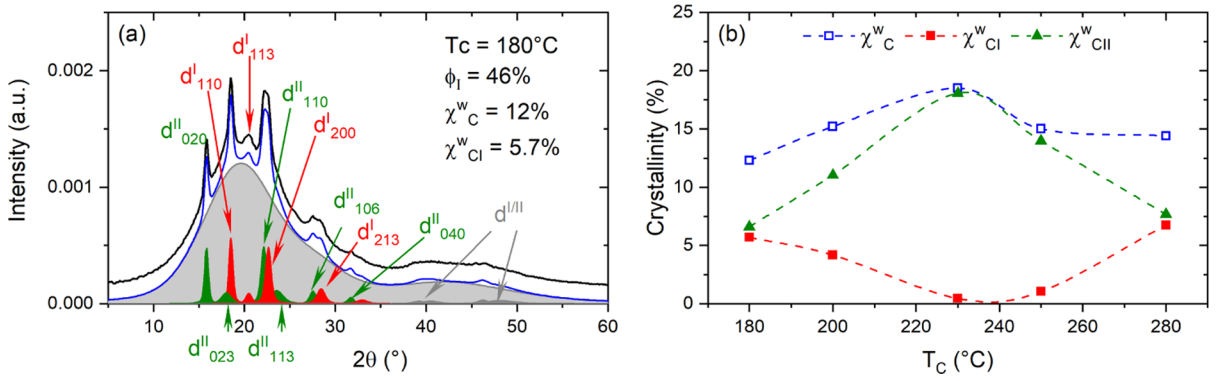

Figure 3. Results of the quantitative analysis. (a) Film cold-crystallized at T_C = 180 °C, amorphous halo in gray, Bragg peaks of form I in red and form II in green, the nonresolved form I/II are in dark gray, and the blue line corresponds to the sum of the amorphous halo and sharp peaks. (b) crystallinities (total and relative to each form I and form II) evolution with T_C. Dotted lines are guides to the eye.

The WAXS spectra evolve significantly with the crystallization temperature. At T_C = 230 °C, PEKK 6002 crystallizes almost exclusively in form II; the amount of form I is very low Φ_I = 2%, and the sample has the highest crystallinity, χ_c^w = 18.5% (χ_{cI}^w = 0.4% and χ_{cII}^w = 18.1%). For T_C = 180 and 280 °C, the amount of form I is around 46%. The lowest crystallinity is measured for the lowest crystallization temperature, 180 °C, χ_c^w = 12%.

3.1.2. Absolute Crystallinity Deduced from the Ruland Method. Published by Ruland in 1961,[33] the first method of absolute measurement of the polymer crystallinity was only applied to a limited number of polymers.[43,48,49] The idea developed in this method is that even if the crystalline and amorphous contributions of the WAXS spectrum can be separated, their respective intensities cannot be unambiguously attributed to the crystalline and amorphous weight fractions because atomic thermal vibrations and lattice imperfections reduce the Bragg peaks intensity and increase the amorphous diffusion. The Ruland method endeavors to take into account these crystalline intensities lost in the amorphous diffusion by introducing a contribution of the disorder. The absolute crystallinity is calculated from the following relation

$$X_c^{abs} = R \times K \text{ with } R = \frac{\int_0^\infty s^2 I_c(s)\,ds}{\int_0^\infty s^2 I(s)\,ds}$$

$$\text{and } K = \frac{\int_0^\infty s^2 \overline{f^2(s)}\,ds}{\int_0^\infty s^2 \overline{f^2(s)}\,D(s)\,ds}$$

where s is the reciprocal space vector ($s = 2\frac{\sin\theta}{\lambda}$).

R is a ratio of two experimental intensities, $I(s)$ is the coherent intensity obtained after normalization in absolute units and subtraction of the calculated incoherent intensity, and $I_c(s)$ is the crystalline peak intensity extracted from $I(s)$ (details in the Supporting Information).

K is calculated from $\overline{f^2(s)}$ (the weighted mean-square atomic scattering factor: $\overline{f^2(s)} = \frac{\sum N f_i^2}{\sum N_i}$) and D is the disorder function ($D(s) = \exp(-ks^2)$). In this expression, k includes the effect of thermal motion as well as lattice imperfections in general.[33]

The computation of the coherent and incoherent intensities, then the integrations and normalization, must be done from a lower limit s_0 to an upper limit s_p in a large region of s. For a series of integration intervals (fixed s_0 and various s_p), the equation $X_c^{abs} = R \times K$ can be solved by determining the series of $K(s_p)$ values, which yields X_c^{abs} constant for a given D function (k value).[33,48,49] The interval used by Ruland is $[s_0 - s_p] = [0.1 - 1.25]$, it corresponds to $2\theta \in [9, 150°]$ for copper radiation. This very large required angular range explains why this method is not easily and commonly used.

The Ruland method was then simplified, adapted to a smaller 2θ range [5, 60°], and applied to other polymers.[43,50,51] Instead of solving the equation $X_c^{abs} = R \times K$ for various integration intervals and various k values, Vonk proposed a graphical method where $1/R(s_p)$ is plotted versus s_p^2. This curve should oscillate around the straight line defined by[43,51]

$$y = \frac{1}{X_c^{abs}} + \frac{1}{2}\frac{k}{X_c^{abs}} \times s_p^2$$

As already mentioned, the acquisition of WAXS spectra with the wide s range used by Ruland and Vonk is not easy to achieve experimentally. Nevertheless, crystallinity can be estimated with reasonable accuracy using the limited s range [0.1–0.66] that corresponds to $2\theta \in [9, 60°]$ with the copper radiation.[50,51] In this work, as the angular range is [5, 62°], the same approximation was applied and X_c^{abs} and k were calculated for the PEKK films used herein. The results are gathered in Table 2. The procedure used in the present study is described

Table 2. Quantitative Data Deduced from WAXS Analysis: Crystallinity χ_c^w and Form I Fraction Φ_I from the Peak-Fitting Method and X_c^{abs} and k from the Ruland and Vonk–Ruland methods

	peak-fitting WAXS method		Ruland method[33,48]		Vonk–Ruland method[43] (graphical method)	
crystallization conditions[a]	χ_c^w	Φ_I	X_c^{abs}	k	X_c^{abs}	k
CC180	0.12	0.46	0.105	1.9	0.115	3.1
CC200	0.15	0.28	0.14	2.6	0.15	3.8
CC230	0.185	0.02	0.17	2.7	0.18	3.8
CC250	0.15	0.07	0.14	2.4	0.15	3.6
CC280	0.14	0.47	0.11	1.6	0.12	2.5
MC280	0.11	1.0	0.11	1.7	0.12	2.5
CC280[b]	0.10	0.95	0.09	0.9	0.10	1.35

[a]Crystallization conditions: CC for cold crystallization and MC for melt crystallization. [b]Sample cold-crystallized at 280 °C after a heating ramp of 50 °C/min to reach 280 °C (See Figure 4).

and illustrated in the Supporting Information (Figure S2 and Table S1). Even if the k values estimated from the two methods[33,43] are not exactly the same, their evolutions as a function of T_C are similar. The highest k values are observed for the crystallization temperatures around 200−230 °C. The crystallinity calculated with the Ruland method[33] is slightly lower than with the Vonk−Ruland method.[43]

Crystallinities measured with the three methods are very similar (Table 2 and Figure S3), although they originate from different calculations. In all methods, WAXS spectra are acquired in the same angular range (relatively large). However, in the peak-fitting method, contrary to the Ruland method, polarization, absorption, and Lorentz corrections were not applied. In addition, WAXS spectra were not normalized in absolute units and the incoherent diffusion was not subtracted. Only a linear baseline was subtracted, and the crystalline and amorphous contributions were separated by fitting the whole WAXS spectra with broad and sharp peaks. Constraints were applied on the broad peaks to control the shape of the amorphous phase and on the sharp peaks in agreement with the cell parameters and to maintain the intensity ratio and width of some specific Bragg peaks as much as possible. Besides its ease of use, the peak-fitting method, even if it is not ≪absolute≫, also provides the relative amount of each crystalline form, I and II, as well as their interplanar distances. Their cell parameters can thus be deduced.

Regardless of the method used for the crystallinity calculation, values between 11 and 19% are measured. These values are low compared to the crystallinity deduced from DSC measurement[29] for the PEKK copolymer with the same T/I ratio (60/40) (around 20−28%) or from WAXS for PEEK (26−32%)[52] and PEKK (22−35%).[47] Comparison with DSC measurements will be discussed later. In WAXS experiments, differences in the calculated weight crystallinity with values read in the literature are mainly due to the angular range (2θ) used for this calculation. In PEEK and PEKK literature studies,[52,47] the often-used angular range [10, 35°] is very narrow compared to the very wide range [8, 150°] used in the Ruland method. In the present study, the integrated intensities, A_c and A_t, were calculated over a relatively wide 2θ range, from 5 to 60°, with a linear subtracted baseline, defined at the intensity level at 5 and 60°. In this range, all of the sharp diffraction lines and the three amorphous broad lines were taken into account; the crystallinity was thus calculated as 18.5% (T_C = 230 °C, Figure 2b). Considering the 2θ range [10, 35°] used in the literature and a baseline defined at the limits of this restrained domain, the calculated crystal ratio is 27%, which is significantly overestimated due to an under-estimation of the amorphous contribution. This value is comparable to the crystallinity measured on PEEK[52] (27%) and PEKK[47] (26%) for the same 2θ range [10, 35°]. Discussion on the relationship between the angular range, baseline, and crystallinity, is reported in the Supporting Information (Figure S4).

3.2. Heating Rate to the Crystallization Temperature.

As it has been shown previously, the crystallization process of PEKK significantly influences the final crystalline structure, i.e., form I or form II. In the literature, this point is qualitatively reported for the three main crystallization methods: crystallization from the melt, cold crystallization, and solvent-induced crystallization.[20,22,53] As observed in this study (Figure 2) and also in the literature, form I is often found after melt crystallization, while a mixture of form I and form II is obtained after cold crystallization.[20] Isothermal crystallization kinetics was also studied for this specific PEKK grade (T/I = 60/40). The crystallization rate is slow with a characteristic time of the order of few minutes. The fastest crystallization is observed at around 230−240 °C.[22,54]

In Section 3.1, crystallizations were conducted in a ventilated oven with a moderate heating rate (around 15 °C/min) to reach T_C. To simulate the heating up, DSC traces were recorded on amorphous films during heating at 10, 20, and 50 °C/min (Figure S5). Significant exotherms were detected above 225 °C during heating at low heating rates, 10 and 20 °C/min (Figure S5), but no crystallization peak was observed below 225 °C. Crystallization in the ventilated oven during heating up to 180, 200, and 230 °C can then be ruled out. However, for higher temperatures, typically 280 °C, a possible crystallization during heating can be suspected. To study the effect of the heating rate on the form I/form II composition, the samples crystallized at 230 °C (and 280 °C) in the DSC oven were also prepared. The isotherm at 230 °C (and 280 °C) in the DSC oven was limited to 4 h (instead of 24 h in the ventilated oven) and various heating rates, from 5 to 50 °C/min, were applied to reach T_C. The crystallized samples were taken out of the DSC pan and analyzed with X-ray to quantify the amounts of form I and form II. The results are reported in Supporting Information Figure S6. As expected, the crystallization at 230 °C was not significantly affected by the heating rate to reach the crystallization temperature. Less than 3% of form I was measured regardless of the protocol used. On the other hand, for samples crystallized 4 h at 280 °C, the relative amount of form I increases from 18 to 95% for heating rates ranging from 5 to 50 °C/min. For low heating rates, 20 °C/min and lower, the samples crystallize during heating, while at 50 °C/min, no significant crystallization appears during heating (also observed in Figure S5). Thus, the significant amount of form II obtained for the heating rate lower than 50 °C/min was due to the high crystallization rate of form II at around 240 °C for cold crystallization.[54] If the amount of form I obtained after the crystallization in the oven at 280 °C is reported on the graph of Figure S6, the heating rate can be deduced and estimated around 15 °C/min. This heating rate estimation appears consistent with the protocol used (see the Section 2) and explains why a high amount of form II was observed after cold crystallization at high temperatures (Figure 3b). Tuning the heating rate to reach a crystallization temperature as high as 280 °C is a simple way to promote the crystallization into a mixture of form I and form II with a well-defined amount of each form (Figure 4).

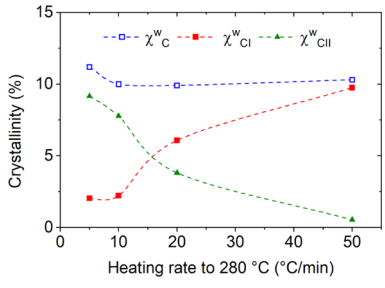

Figure 4. Crystallinities, total and relative to form I and form II, versus the heating rate to reach the cold-crystallization temperature T_C = 280 °C. Dotted lines are guides to the eye.

3.3. Crystalline Lamellae, SAXS Spectra. SAXS spectra for all of the films are reported in Figure 5a. Apart from the as-received film, a correlation peak for all of the crystallized films is observed. This unique peak reveals a periodic organization between the two phases of significantly different electron densities. The respective densities of the two crystal form I and form II are very close (1.35 and 1.38 g/cm^3, respectively), calculated from the two volumes of crystal cells (1477 and 1438 Å^3 for form I and form II, respectively, according to Table 1). On the other hand, these densities differ significantly from the amorphous density measured at 1.27 g/cm^3.[35] Thus, the correlation peak observed in Figure 5a must be due to the difference in density between the crystalline lamellae and the amorphous phase. However, the nature of the crystalline lamellae (form I and/or form II) cannot be discriminated. This peak, which is characteristic of the periodic organization of the crystalline lamellae, evolves in position and shape with T_C. From these spectra, the correlation function of the electronic density $K(z)$ was calculated. The long period L_P was deduced from the position of the first maximum of $K(z)$, and the thickness of the crystalline lamellae L_C was measured at the intersection between the two tangents, as shown in Figure 5b, for the film crystallized at T_C = 230 °C. The evolutions of L_P and L_C are reported in Figure 5c. At first, the increase of the long period L_P, as a function of T_C, is slow (from 110 Å at T_C = 180 to 120 Å at T_C = 230 °C), then more pronounced up to 170 Å at T_C = 280 °C. On the other hand, the thickness of the crystalline lamellae, L_C, increases slowly from 24 to 39 Å in the whole T_C range. L_C corresponds to the crystal size along the chain direction. The ratio of these two lengths, L_C/L_P, corresponds to the overall volume crystal ratio provided that all of the amorphous phases is located between the crystalline lamellae periodically organized. The thickness of this amorphous interlayer is $L_a = L_P - L_C$. This thickness evolves from 86 to 131 Å. The ratio L_C/L_P (Figure 5c) and the weight crystallinity χ_c^w (Figure 3b) appear to evolve similarly. This point will be discussed later.

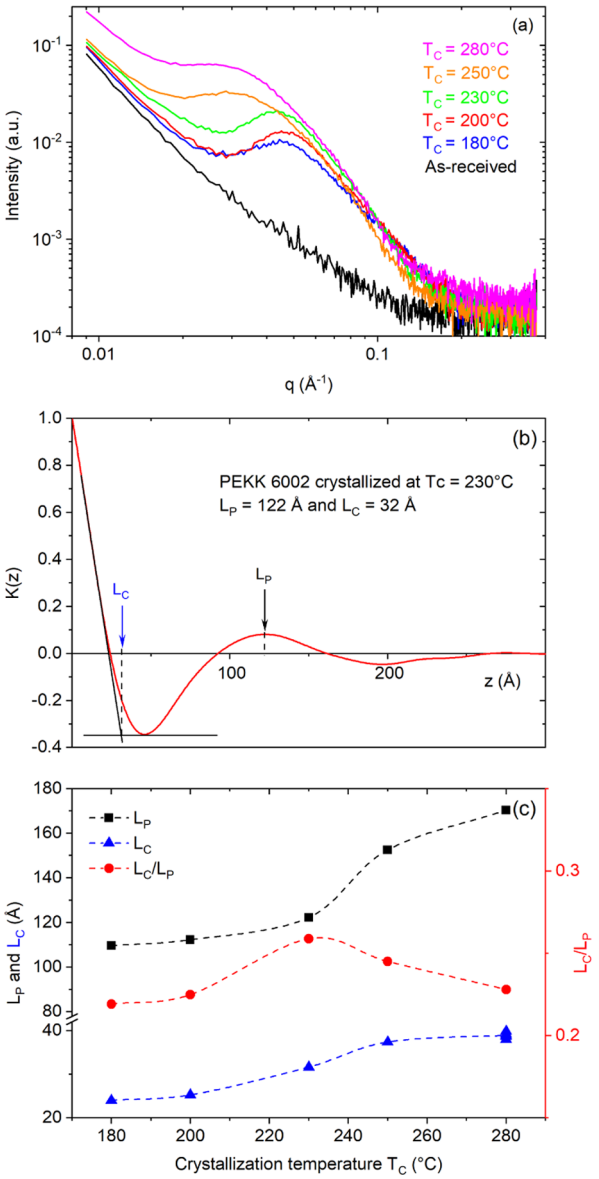

Figure 5. SAXS data for the different crystallization temperatures T_C. (a) Superposition of the SAXS spectra in the logarithmic scale. (b) Correlation function of the electronic density $K(z)$ for T_C = 230 °C with the determination of L_P and L_C. (c) Long period L_P (black square solid), crystalline lamellar thickness L_C (blue triangle up solid), and the ratio L_C/L_P (red circle solid) for T_C from 180 to 280 °C. Dotted lines in (c) are guides to the eye.

3.4. Melting of the Crystalline Phases, DSC. Another classical way to study the crystalline state of the films is by thermal analysis (DSC experiments). First heating traces recorded with a rate of 10 °C/min are reported in Figure 6 for as-received and cold-crystallized samples. The arrows indicate the crystallization temperature. For all of the crystallized samples, a glass transition T_g was observed at around 160 °C, followed by multiple endotherms.

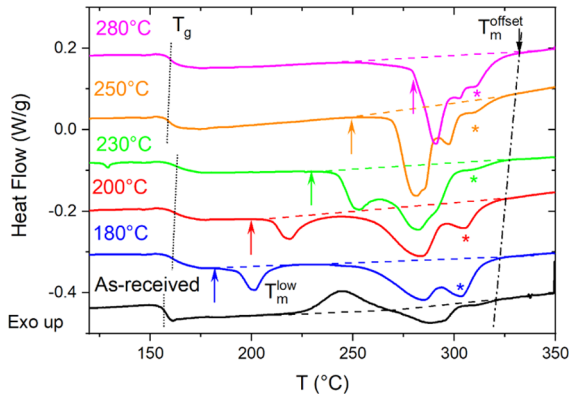

Figure 6. First heating at 10 °C/min recorded on amorphous and cold-crystallized films. The colored arrows indicate the crystallization temperature T_C. On the left, the dotted lines indicate the glass transition T_g. On the right, the dash-dotted line indicates the offset melting temperature, T_m^{offset}. The star (*) indicates the higher temperature contribution of the endotherm, possibly associated with the form I melting (see the Discussion section). Dashed lines are guides to the eye, indicating the baseline used for the enthalpy calculation.

For the as-received amorphous film, the glass transition is measured at 158 °C, an exotherm of crystallization is observed, followed by a melting endotherm. A slight increase of the glass transition is observed for the samples crystallized at 250 and 280 °C, with respective values of 159 and 160 °C. This increase is more pronounced for lower T_C, glass transition temperatures at 161, 162, and 163 °C are measured for

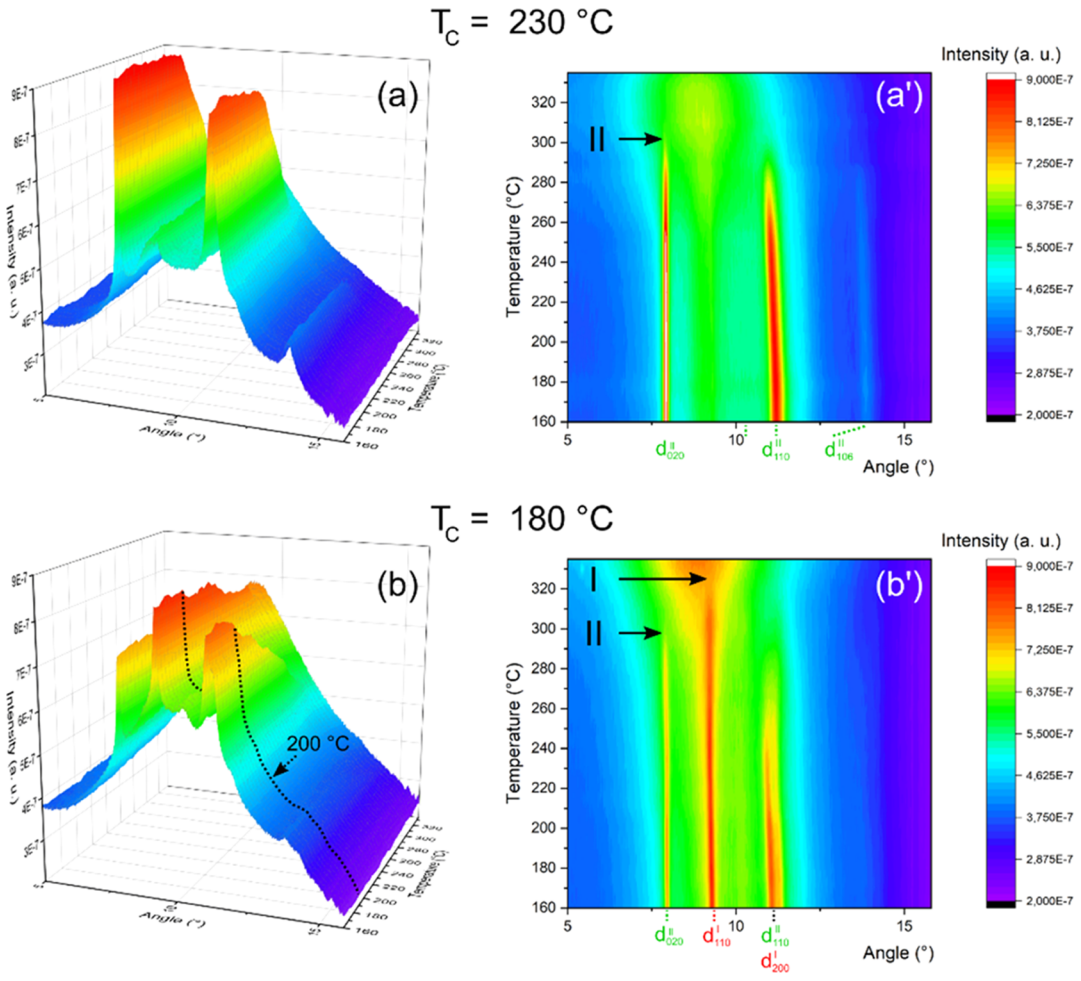

Figure 7. *In situ* WAXS diffraction patterns of PEKK films cold-crystallized at 230 °C (a)−(a′) and 180 °C (b)−(b′) heated between 160 and 335 °C at a heating rate of 10 °C/min. In the 2D representations (a′) and (b′), the arrows indicate the melting offset of the two crystalline forms, form I and form II.

respective crystallization temperatures of 180, 200, and 230 °C. T_g seems to be maximum for crystallization at 230 °C ($T_g^{\text{amorphous film}}$ + 5 °C). This may be due to the faster crystallization kinetics at this temperature.[22,54] This increase of T_g for the crystallized films, as compared to the amorphous one, has already been observed for PEKK.[47] It is attributed to the constraints imposed by the crystalline lamellae on the amorphous chain mobility. This positive offset decreases with the increasing crystallization temperature as reported for various PEKK with the T/I ratio 100/0, 70/30, and 60/40.[47]

For crystallization at T_C = 180 and 200 °C, a small and well-defined melting endotherm is detected at T_C + 20 °C. The temperature of this endotherm named T_m^{Low} will be discussed later in the Section 4. At higher temperatures, a double endotherm with respective minima at around 283 and 305 °C was observed. For higher T_C, the small endotherm at T_m^{Low} merges with the high-temperature melting endotherm. The shape of the melting endotherm is completely modified for $T_C \geq 230$ °C. Regardless of its shape, the end of the endotherm at high temperatures defines an offset temperature T_m^{offset} varying from 320 to 330 °C, for T_C varying from 180 to 280 °C.

Since the WAXS study of these films evidenced their polymorphism (crystalline form I and form II), it was interesting to qualitatively identify the contribution of each crystalline form to the melting endotherm. To this end, *in situ* WAXS experiments were performed during a heating ramp at the same heating rate as in DSC (10 °C/min). These experiments were run at the Soleil synchrotron facility (Saclay, France).

3.5. Melting of the Crystalline Phases, *In Situ* WAXS. Two films, cold-crystallized at 230 and 180 °C, having different polymorphic compositions to assess the different melting endotherms of the crystalline forms were selected. Figure 7 shows the evolution of the diffraction patterns of these films between 160 and 335 °C (three-dimensional, 3D representation in (a) and (b) and 2D projection in (a′) and (b′)). Due to the beamline wavelength used to collect these WAXS spectra, the Bragg peaks are at scattering angle positions at roughly half the position detected with the Cu Kα radiation. On these spectra, it is noteworthy that two peaks are singular for the two forms (d^{II}_{020} at 2θ = 7.8° for the form II and d^{I}_{110} at 2θ = 9.3° for the form I). The 230 °C film shows only characteristic peaks of form II, whereas the 180 °C film shows both form I and form II peaks.

As the temperature increases, the intensity of all of the peaks remains more or less constant for a certain temperature range and then it starts to decrease to reach the amorphous state, identified by a wide halo. A single plateau is clearly observed in Figure 7a, while two stages are observed in Figure 7b, the slight decrease of the Bragg peak intensities observed at 200 °C for

the film crystallized at 180 °C is probably associated with the low melting endotherm observed at 200 °C in this sample. In Figure 7a′, for the film crystallized at 230 °C, the Bragg peaks associated with the form II totally disappear at ca. 300 °C. A similar melting behavior can be detected for the film crystallized at 180 °C in Figure 7b′, where form II peaks disappear at ca. 295 °C (the d_{020}^{II} peak), while the peak of form I, $d_{100,}^{I}$ disappears at higher temperatures, ca. 320 °C. The slight difference (less than 5 °C) in the offset melting temperature of the d_{020}^{II} peak between the 180 and 230 °C films may be due to the difference in the lamellar thickness of the form II crystals in these two films. This point will be discussed in the last part of the Section 4. These data indicate that the form II melts at lower temperatures than the form I and that there is no transition of form II to form I for these cold-crystallized PEKK materials.

4. DISCUSSION

Up to now, it was shown that starting with an amorphous sample of PEKK and using a ventilated oven, PEKK can crystallize at various crystallinities and various amounts of form I and form II. The crystalline structure and the lamellae morphology were characterized using WAXS, DSC, and SAXS. Applying the peak-fitting quantification method to WAXS spectra, the total weight crystallinity χ_c^w as well as the crystallinity of each crystalline form were thoroughly quantified. Data on the evolution of crystal lattices were also obtained. The next section will be focused on the global analysis of WAXS, SAXS, and DSC experiments, which can lead to precise and important information on the structure and morphology of PEKK. This includes the interpretation of the various melting temperatures and the calculation of the melting enthalpy $\Delta H_m^{100\%}$ of a 100% crystallized PEKK. The evolution of the cell parameters (form I and form II), the absolute crystallinity χ_c^w, the crystalline lamellar thickness (L_C), and periodicity (L_P) with T_C will be quantified and discussed.

4.1. Melting Temperatures of the Two Crystalline Forms (WAXS and DSC). Melting endotherms with multiple peaks observed for this PEKK copolymer are intricate to interpret. In the temperature range from the glass transition (around 160 °C) to 350 °C, almost three endotherms can be identified.

The first one appears approximately 20 °C above the crystallization temperature. This small lower temperature endotherm is largely reported and studied for PEEK[52,55−57] and PEKK.[22,29] Although widely studied, its origin is not yet established even if various interpretations were advanced, e.g., the melting of a secondary structure within the spherulite[22,29] or the melting and reorganization of thin crystalline lamellae.[52,55,56] More recently, Marand et al. demonstrated that the multiple melting phenomena observed in PEEK are not explained by the melting−recrystallization−remelting concept but by the melting of secondary crystals.[57] These inter-lamellar secondary crystals appear in the constrained amorphous phase after annealing above the glass transition. They are described as bundled chain crystals (or fringed micellar crystals) of limited lateral dimensions. Interesting correlations between the small crystal formation and the "physical aging" observed after annealing below the glass transition were discussed by the same authors.[58] Their interpretations are based on DSC experiments, specifically on the effect of the heating rate on the melting behavior of melt and cold-crystallized PEEK.[57] The heating rate dependence of the low endotherm temperature (T_m^{Low}) is the same for melt and cold-crystallized samples: T_m^{Low} increases with the heating rate. On the other hand, the temperature of the high endotherm, T_m^{High}, decreases for the cold-crystallized samples, while it remains unaffected for the melt-crystallized sample. They concluded that the low and the high-temperature endotherms are associated with different populations of crystals and that the evolution of T_m^{High} after cold crystallization suggests the melting−recrystallization−remelting process during heating.

For PEKK, the melting endotherm, at higher temperatures, is not a single peak as it is for PEEK but a double one, and hence, the three endothermic peaks are observed in Figure 6. The thermogram of the sample cold-crystallized at 200 °C exhibits three well-defined endotherms. A heating rate study, according to Marand et al.,[57] was performed on this sample to explain and identify the multiple endotherms of PEKK. Heating traces at various heating rates are reported in Figure S7. When the heating rate was increased from 2.5 to 40 °C/min, a significant increase of T_m^{Low} (Figure S7) was observed along with a decrease of the temperature of the double high-temperature endotherm (Figures S7 and S8b). The two components of this high-temperature endotherm evolved in the same way with the heating rate, which can be interpreted by a reorganization during heating of two independent crystalline forms (form I and form II) without clear evidence of a transition between these two crystalline forms. The dependences of the low melting temperature, T_m^{Low}, with the heating rate and the crystallization time are reported in Figure S8a,c. These two evolutions of T_m^{Low} are close to those observed by Marand et al.[57] for PEEK. It was thus concluded that the first endotherm peaks located at T_m^{Low} in PEKK are associated with the melting of secondary fringed micellar crystals formed during the crystallization process in the constrained amorphous phase. The small abrupt decrease of intensity observed in Figure 7b, and highlighted by the black dotted line, could be associated with the melting of these secondary crystals. On the other hand, the high-temperature double endotherm is associated with the melting of the primary crystals. Reminding that form II melts before form I (WAXS *in situ* experiments Figure 7), we propose that the first high-temperature endotherm (around 280 °C) is mainly associated with the melting of form II, while the second one (around 290 °C) is associated with the melting of form I.

The spatial distribution of crystal form I and form II within crystal lamellae remains uncertain. It is not known whether the two crystal forms, form I and form II, coexist in each lamella or whether crystalline lamellae of each form coexist. In the same way, it is not obvious to precisely separate the contributions of form I and form II in the high-temperature double endotherm and to extract their relative fractions. Figure S9 compares the DSC traces of PEKK crystallized in form II (CC at T_C = 230 °C) and form I (MC at T_C = 280 °C), while WAXS spectra, of these two samples, are reported in Figure 2b,d. The melting endotherms of each pure crystalline form show a multiple peak behavior in the same temperature range, around 290 °C (Figure S9). For films cold-crystallized at higher temperatures, e.g., 250 and 280 °C, the shape of the endotherm is even more complex as it incorporates the low-temperature endotherm peak. It seems reasonable, however, to associate the part of the endotherm marked with a star in Figure 6 with the melting of the form I. Indeed, this part of the endotherm seems to evolve in the same way as the amount of form I deduced from the

WAXS experiments (Figure 3b). All of these data (DSC and WAXS) confirm that form I is more stable than form II.[22,23]

Differences in the phenyl−phenyl interactions between the closest chains in the different crystals are reported in the literature, with edge-to-face interactions in form I and face-to-face in form II.[22] The energy differences that depend on the substituent are not easy to estimate between the perpendicular and parallel cycle stacking.[59] Distances between the closest chains in the two crystal forms, form I and form II, are significantly different ($(a^2 + b^2)^{1/2} \sim 4.9$ Å in form I and $a \sim 4.2$ Å in form II, see Figure S1) and they have an impact on the respective perpendicular and parallel cycle stacking energies. It is thus not obvious that this kind of argument can explain the thermal stability of the two crystalline forms.

4.2. Crystallinity Evolution (WAXS, SAXS, and DSC). In a semicrystalline polymer, SAXS, WAXS, and DSC are often used to study the fraction of the crystalline phase. With SAXS, the periodic organization of the crystalline lamellae can be observed and the period L_P can be measured. Using the model developed by Strobl and the calculation of the electron density correlation function,[45] the thickness L_C of the crystalline lamellae can then be deduced. L_C/L_P corresponds to the volume ratio of the crystalline lamellae in the lamellar stacks. This ratio can be compared to the volume crystalline fraction if the entire amorphous phase is located in the lamellar stacks. Using the diffraction spectra recorded through WAXS, the crystal structure was deduced and the weight crystallinity χ_c^w, which depends on the weight of atoms organized in the crystalline planes, was calculated. L_C/L_P and χ_c^w are reported in Figure 8 for the various T_C. They were measured at room temperature and they should obey the following relationship

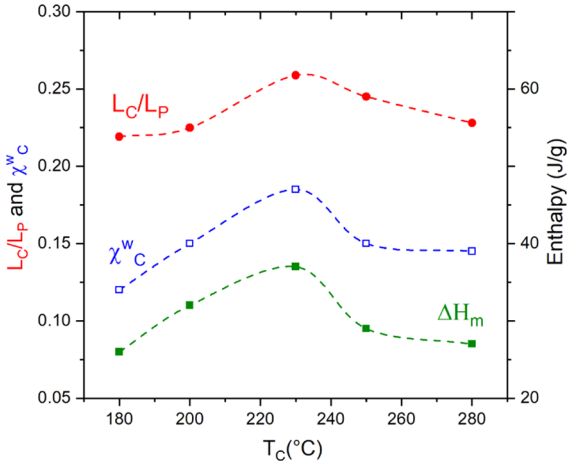

Figure 8. Various crystal parameters, L_C/L_P from SAXS, χ_c^w from WAXS, and ΔH_m from DSC as a function of T_C. Dotted lines are guides to the eye.

$$(L_C/L_P) = (\rho/\rho_c)\cdot\chi_c^w$$

where ρ is the electronic density of the whole material (including both amorphous and crystalline fractions) and ρ_C is the electronic density of the crystalline phase. As the material is not fully crystallized, the following inequality stands: $\rho/\rho_c < 1$. Yet, in Figure 8, it is shown that $L_C/L_P > \chi_c^w$ regardless of the crystallization temperatures. This is an indication that the amorphous phase is also located outside of the lamellar stacks, either as amorphous pockets between bundles of lamellae within the spherulites, as often observed in polymer blends[60,61] or as the interspherulitic amorphous phase. L_C/L_P measures the volume crystallinity inside the lamellar stacks, which should not be considered as a macroscopic value for the entire sample.

With the DSC experiments upon the first heating, the enthalpic signals, exotherm, and endotherm were measured and associated with the crystallization and the melting of the crystalline content, respectively. As previously discussed, the endothermic event is broad, from T_C + 20 to 320 °C. The integration of the endotherm corresponds to the enthalpy, ΔH_m, required to melt the amount of crystalline phases that exist at the melting onset, consisting of all of the crystals, secondary and primary, and both crystalline forms, form I and form II. In Figure 8, the evolution of ΔH_m with T_C is reported.

These three sets of data, L_C/L_P, χ_c^w, and ΔH_m, evolve in a similar way with the crystallization temperature (Figure 8). They show a maximum at around 230 °C, meaning that the crystallization efficiency is optimal at this temperature.

From these data, the melting enthalpy $\Delta H_m^{100\%}$ of a 100% crystallized PEKK can be calculated. Although the use of this quantity, $\Delta H_m^{100\%}$, to calculate crystallinity from DSC measurements is debatable,[62−64] it is widely used. Indeed, one of the critical points is that the crystalline state of the polymer (thickness of lamellae, crystallinity, density, etc.) just before melting is not necessarily the same as that of the polymer at room temperature at which the densities or crystallinities are measured by WAXS. To the best of our knowledge, no experimental value was published for PEKK. A value of 150 J/g (45 kJ/mol in ref 65) was calculated from molecular dynamics simulations for a PEKK 60/40.[65] However, the only used $\Delta H_m^{100\%}$ values are those published for PEEK.[63,19,66,67] The most often-referred value is 130 J/g,[19] calculated from WAXS (crystallinity estimated in the range $2\theta \in [10, 36°]$, without any correction), density, and DSC experiments. Two higher values of $\Delta H_m^{100\%}$ for PEEK were calculated from two independent methods, 165 J/g, from density and DSC[67] and (161 ± 20) J/g from pressure−volume−temperature (PVT) experiments using the Clapeyron equation.[66]

The $\Delta H_m^{100\%}$ value evaluated in the present work, ∼200 J/g, is the first experimentally estimated value for the PEKK polymer, and this value is obtained through the peak-fitting method on a PEKK 6002 (T/I ratio of 60/40) crystallized in a mixture of form I and form II. Figure S10 compares the $\Delta H_m^{100\%}$ values calculated with the three WAXS treatments used in this study, and values 211 and 226 J/g are calculated with the Ruland methods. It was concluded that a value $\Delta H_m^{100\%}$ = (202 ± 20) J/g is a reliable estimation to calculate the room temperature crystallinity of PEKK 60/40 from DSC measurement.

The PEEK value of 130 J/g was deduced from a WAXS crystallinity calculated without any corrections in a range of $2\theta \in [10, 36°]$.[19] We have shown in Section 3.1 that the use of this restrained 2θ range leads to an overestimation of the crystallinity. Therefore, this often-used 100% melting enthalpy of PEEK (130 J/g) is most probably underestimated. We can speculate that the 100% melting enthalpies of PEEK and PEKK are probably close, around 200 J/g. Specific WAXS and DSC experiments on PEEK are needed to conclude on this point, which is out of the scope of the present study.

4.3. Cell Parameters and Crystallization Temperatures. From the WAXS spectra analysis (Figure 2), the interplanar distances, d_{110}^{I} and d_{200}^{I} of form I and d_{020}^{II} and d_{110}^{II}

of form II, were calculated. Thus, for each crystallization temperature, and using the general expression of d_{hkl}, the cell parameters ≪*a*≫ and ≪*b*≫ of crystalline form I and form II can be calculated. The evolution of these cell parameters with the crystallization temperature T_C is reported in Figure 9.

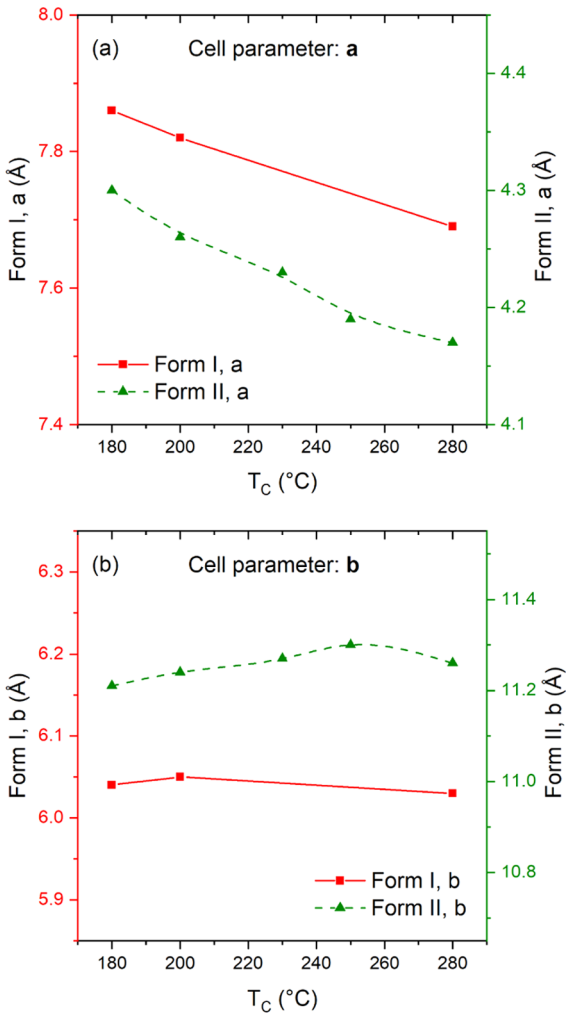

Figure 9. ≪*a*≫ and ≪*b*≫ cell parameters of the crystalline form I and form II for various T_C. For each cell parameter, the full scale represents a relative variation of 8%.

Cell parameters are calculated only for crystalline forms that show an amount greater than 10%. It appears that the ≪*a*≫ parameter is more sensitive to the crystallization temperature than the ≪*b*≫ parameter. The ≪*a*≫ parameter decreases when T_C increases, while the ≪*b*≫ parameter remains almost constant. Anisotropic dimensional changes have been reported for PEEK, PEKK (100% *T*), and PEKK (100% *I*) melt-crystallized in form I. The explanation could be that the chain folding occurs along the ≪*a*≫ direction.[17] As the crystallization temperature increases, the chains would stack closer than at low temperatures since the crystallization would be less chaotic at high temperatures. The ≪*a*≫ parameter would thus decrease, whereas the ≪*b*≫ parameter would be insensitive to this stacking modification. Here, the same evolution for PEKK (*T*/*I* = 60/40) cold-crystallized can be observed, regardless of the crystal form.

4.4. Thickness and Periodicity of the Crystalline Lamellae (SAXS and DSC). In Figure 5c, it is shown that the crystalline lamellar thickness, L_C, increases continuously with the crystallization temperature. In Figure 7, the offset melting temperature of form II crystallized at 180 °C is 5 °C lower than that of the sample crystallized at 230 °C. This temperature shift can be due to the different crystalline lamellar thickness, respectively, 24 and 31 Å measured for T_C 180 and 230 °C (Figure 5c). On the DSC thermograms, a slight increase of the highest melting temperature peak, referred by the star (*), and of the offset melting temperature, T_m^{offset}, with the crystallization temperature (Figure 6), can also be measured. All of these observations are in line with observations reported in the literature for other semicrystalline polymers, which establish a relationship between the isothermal crystallization temperature T_C, the melting temperature T_m, and the thickness of the crystalline lamellae L_C.[68−70] In these publications, the authors have shown that, for solvent or melt-crystallized samples, the thickness of the crystalline lamellae is defined by the crystallization temperature, and a linear relationship is observed between T_C and L_C^{-1}.

In Figure 10, T_C is plotted versus the inverse crystal thickness for all of the crystallization temperatures used. We

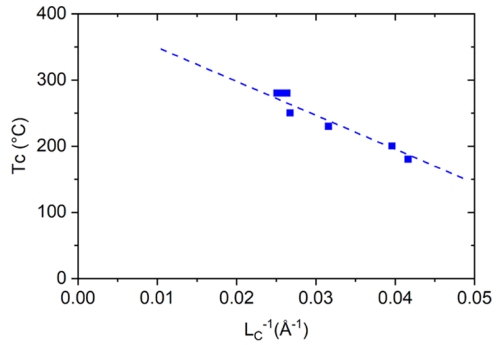

Figure 10. Dependence of the crystallization temperature T_C on the inverse crystalline lamellar thickness, L_C^{-1}. The dotted line is a guide to the eyes.

did not plot the melting line, T_m versus L_C^{-1}, because this latter line must be constructed with the lamellar thickness just before the final melting.[70] This latter data requires to conduct temperature-dependent SAXS experiments that may show a possible lamellar thickening process.

In Figure 10, all of the experimental points, from crystallization either in the ventilated oven or in the DSC oven, seem relatively well aligned, regardless of the crystal form. It is not known whether the two crystal forms coexist in each lamella or whether crystalline lamellae of each form, form I and form II, coexist. But in any case, a linear relationship between T_C and L_C^{-1} is observed for all of the cold-crystallized PEKK samples. It therefore appears that the heating rate to reach the crystallization temperature does not significantly influence the thickness of the crystalline lamellae but defines the nature of the crystalline phases inside these lamellae.

5. CONCLUSIONS

A quantitative structural study of the cold crystallization of amorphous PEKK (*T*/*I* = 60/40) crystallized at various temperatures, ranging from 180 to 280 °C was presented. This study was conducted using SAXS−WAXS and DSC experiments. The formation of crystalline lamellae, with thickness L_C, periodically organized was observed. The thickness of the crystalline lamellae, the crystalline forms nature, and their

amounts evolve with the crystallization temperature. These various structural and morphological states lead to different thermal behaviors observed by DSC.

The peak-fitting method used in this study to analyze the WAXS spectra was described in detail. This method requires the subtraction of a baseline. The choice of the angular domain is therefore critical and it was shown that a relatively wide angular range $2\theta \in [5, 60°]$ is necessary. With this angular range, the calculated total weight crystallinities, χ_c^w, are in very good agreement with the absolute crystallinities deduced from the Ruland method. In addition, contrary to the Ruland method, this peak-fitting method provides quantitative information on each crystalline phase, the weight crystallinities (χ_{cI}^w and χ_{cII}^w), the interplanar distances, and the cell parameters.

Thanks to this quantification method applied to WAXS spectra, significant evolution of Φ_I, from 46 to 2% (χ_{cI}^w from 6 to 0.4%) and of χ_c^w, from 12 to 19%, for crystallization temperatures varying from 180 to 230 °C, was observed. By controlling the heating rate to reach an isotherm at 280 °C (from 5 to 50 °C/min), the amount of form I, Φ_I, can also be monitored (from 20 to 95%). This quantitative result is very important for selecting the nature and the amount of crystalline phases in a PEKK material.

A linear decrease of the inverse crystalline lamellar thickness L_C^{-1} with the decreasing crystallization temperature T_C was observed. This evolution, frequently reported for crystallization from the melt, is observed here for cold crystallization. Moreover, an anisotropy in the cell parameter dependence with T_C was also noticed. This highlights the anisotropic growth of the crystalline lamellae and indicates that the chain folding occurs along the $\ll a \gg$ direction in PEKK (T/I) crystallized in form I and form II, as already observed for form I in PEEK, PEKK(T), and PEKK(I).

From our WAXS and DSC experiments, for the first time, the enthalpy of a 100% crystallized PEKK copolymer (T/I = 60/40) was estimated: $\Delta H_m^{100\%} = (202 \pm 20)$ J/g.

The procedure used for crystallization in a ventilated oven highlights the particular influence of the thermal history and crystallization kinetics on the crystalline forms. This is an important piece of information for applications when the processing time does not allow to reach the required final state of crystallization as, for instance, in injection molding, in powder or extrusion coating, or fused filament fabrication (3D printing). The crystalline forms and overall crystallinity can therefore evolve during subsequent processing steps, thermal treatment, and use at $T > T_g$, inducing evolution in the mechanical properties of PEKK parts.

■ ASSOCIATED CONTENT

Supporting Information

The Supporting Information is available free of charge at https://pubs.acs.org/doi/10.1021/acsapm.0c01380.

Details on the calculation of ϕ_I from the WAXS spectra; corrections of WAXS spectra and calculation of normalized intensity in absolute units with Figures S1, S2, and Table S1; details on the crystallinity calculation from the WAXS peak-fitting method with Figures S3 and S4; influence on the heating rate from 20 °C to the crystallization temperature with Figures S5 and S6; complementary DSC experiments for a better understanding of the multiple melting endotherm with Figures S7−S9; correlation between melting enthalpy from DSC and crystallinity from WAXS with Figure S10 (PDF)

■ AUTHOR INFORMATION

Corresponding Author

Sylvie Tencé-Girault − *Laboratoire PIMM, Arts et Metiers Institute of Technology, CNRS, Cnam, HESAM Universite, 75013 Paris, France; Arkema, CERDATO, 27470 Serquigny, France;* orcid.org/0000-0001-5090-2334; Email: sylvie.girault@ensam.eu

Authors

Jonathan Quibel − *Laboratoire PIMM, Arts et Metiers Institute of Technology, CNRS, Cnam, HESAM Universite, 75013 Paris, France*

Alexis Cherri − *Laboratoire PIMM, Arts et Metiers Institute of Technology, CNRS, Cnam, HESAM Universite, 75013 Paris, France*

Sébastien Roland − *Laboratoire PIMM, Arts et Metiers Institute of Technology, CNRS, Cnam, HESAM Universite, 75013 Paris, France*

Bruno Fayolle − *Laboratoire PIMM, Arts et Metiers Institute of Technology, CNRS, Cnam, HESAM Universite, 75013 Paris, France*

Stéphane Bizet − *Arkema, CERDATO, 27470 Serquigny, France*

Ilias Iliopoulos − *Laboratoire PIMM, Arts et Metiers Institute of Technology, CNRS, Cnam, HESAM Universite, 75013 Paris, France*

Complete contact information is available at: https://pubs.acs.org/10.1021/acsapm.0c01380

Notes

The authors declare no competing financial interest.

■ ACKNOWLEDGMENTS

This work was partially funded by the French National Research Agency (ANR IMPEKKABLE project, ANR-15-CE08-0016), authors concerned: J.Q., S.R., B.F., and S.B. This research was also partially carried out within the framework of the Industrial Chair Arkema (Arkema/CNRS-ENSAM-Cnam, Arkema No. AC-2018-413), authors concerned: S.T.-G., A.C., and I.I. Sylvie Lebreton and François Bargain are warmly thanked for their kind welcome and for facilitating SAXS−WAXS experiments at the LEM laboratory, Arkema, Serquigny. We also thank Mahdi Moghaddam for the sample preparation. We thank the SOLEIL synchrotron facility and the SWING beamline for access to the instrumentation and assistance during the *in situ* WAXS experiments (project no 20170187). More particularly, Javier Perez (beamline manager) and Thomas Bizien (beamline scientist) are gratefully acknowledged. Pierre-Antoine Albouy from LPS (Université Paris-Saclay) is warmly thanked for many fruitful discussions on quantitative analysis of the WAXS data.

■ REFERENCES

(1) Schultz, J. M. *Polymer Crystallization: The Development of Crystalline Order in Thermoplastic Polymers*; Université du Michigan: American Chemical Society, 2001.

(2) Cheng, S. Z. *Phase Transitions in Polymers: The Role of Metastable States*; Elsevier Science, 2008.

(3) Tang, X.; Chen, W.; Li, L. The Tough Journey of Polymer Crystallization: Battling with Chain Flexibility and Connectivity. *Macromolecules* **2019**, *52*, 3575−3591.
(4) Chandran, S.; Baschnagel, J.; Cangialosi, D.; Fukao, K.; Glynos, E.; Janssen, L. M. C.; Müller, M.; Muthukumar, M.; Steiner, U.; Xu, J.; Napolitano, S.; Reiter, G. Processing Pathways Decide Polymer Properties at the Molecular Level. *Macromolecules* **2019**, *52*, 7146−7156.
(5) Strobl, G. R. Metastable Partially Crystalline States. In *The Physics of Polymers*; Springer-Verlag: Berlin Heidelberg, 1996.
(6) Lovinger, A. J. Twisted Crystals and the Origin of Banding in Spherulites of Semicrystalline Polymers. *Macromolecules* **2020**, *53*, 741−745.
(7) Lovinger, A. J. Poly(vinylidene Fluoride). In *Developments in Crystalline Polymers-1*; Applied Science Publishers, 1982; pp 195−273.
(8) Chatani, Y.; Shimane, Y.; Inoue, Y.; Inagaki, T.; Ishioka, T.; Ijitsu, T.; Yukinari, T. Structural study of syndiotactic polystyrene: 1. Polymorphism. *Polymer* **1992**, *33*, 488−492.
(9) Kohan, M. I. *Nylon Plastics Handbook*; Hanser/Gardner Publication: Cincinnati, 1995.
(10) De Rosa, C.; Auriemma, F.; Ruiz de Ballesteros, O. A Microscopic Insight into the Deformation Behavior of Semicrystalline Polymers: The Role of Phase Transitions. *Phys. Rev. Lett.* **2006**, *96*, No. 167801.
(11) Auriemma, F.; De Rosa, C.; Esposito, S.; Mitchell, G. Polymorphic Superelasticity in Semicrystalline Polymers. *Angew. Chem., Int. Ed.* **2007**, *46*, 4325−4328.
(12) D'Aniello, C.; Rizzo, P.; Guerra, G. Polymorphism and mechanical properties of syndiotactic polystyrene films. *Polymer* **2005**, *46*, 11435−11441.
(13) Shen, L.; Phang, I. Y.; Liu, T. Nanoindentation studies on polymorphism of nylon 6. *Polym. Test.* **2006**, *25*, 249−253.
(14) Pepin, J.; Gaucher, V.; Lefebvre, J.-M.; Stroeks, A. Biaxial stretching behavior as a probe of H-bond organization in semi-crystalline polyamides. *Polymer* **2016**, *101*, 217−224.
(15) Cocca, M.; Di Lorenzo, M. L.; Malinconico, M.; Frezza, V. Influence of crystal polymorphism on mechanical and barrier properties of poly(L-lactic acid). *Eur. Polym. J.* **2011**, *47*, 1073−1080.
(16) Le, G.; Jouanneau, J.; Clair, N. Process for Producing Polyether Ketone Ketone. EP Patent EP3,438,085A12019.
(17) Cheng, S. Z. D.; Ho, R.-M.; Hsiao, B. S.; Gardner, K. H. Polymorphism and crystal structure identification in poly(aryl ether ketone ketone)s. *Macromol. Chem. Phys.* **1996**, *197*, 185−213.
(18) Dawson, P. C.; Blundell, D. J. X-ray data for poly(aryl ether ketones). *Polymer* **1980**, *21*, 577−578.
(19) Blundell, D. J.; Osborn, B. N. The morphology of poly(aryl-ether-ether-ketone). *Polymer* **1983**, *24*, 953−958.
(20) Gardner, K. H.; Hsiao, B. S.; Faron, K. L. Polymorphism in poly(aryl ether ketone)s. *Polymer* **1994**, *35*, 2290−2295.
(21) Blundell, D. J.; Newton, A. B. Variations in the crystal lattice of PEEK and related para-substituted aromatic polymers: 2. Effect of sequence and proportion of ether and ketone links. *Polymer* **1991**, *32*, 308−313.
(22) Gardner, K. H.; Hsiao, B. S.; Matheson, R. R.; Wood, B. A. Structure, crystallization and morphology of poly (aryl ether ketone ketone). *Polymer* **1992**, *33*, 2483−2495.
(23) Ho, R.-M.; Cheng, S. Z. D.; Hsiao, B. S.; Gardner, K. H. Crystal Morphology and Phase Identifications in Poly(aryl ether ketone)s and Their Copolymers. 1. Polymorphism in PEKK. *Macromolecules* **1994**, *27*, 2136−2140.
(24) Ho, R.-M.; Cheng, S. Z. D.; Hsiao, B. S.; Gardner, K. H. Crystal Morphology and Phase Identification in Poly(aryl ether ketone)s and Their Copolymers. 3. Polymorphism in a Polymer Containing Alternated Terephthalic Acid and Isophthalic Acid Isomers. *Macromolecules* **1995**, *28*, 1938−1945.
(25) Benedetti, L.; Brulé, B.; Decreamer, N.; Evans, K. E.; Ghita, O. R. Shrinkage behaviour of semi-crystalline polymers in laser sintering: PEKK and PA12. *Mater. Des.* **2019**, *181*, No. 107906.
(26) Peyre, P.; Rouchausse, Y.; Defauchy, D.; Régnier, G. Experimental and numerical analysis of the selective laser sintering (SLS) of PA12 and PEKK semi-crystalline polymers. *J. Mater. Process. Technol.* **2015**, *225*, 326−336.
(27) Donadei, V.; Lionetto, F.; Wielandt, M.; Offringa, A.; Maffezzoli, A. Effects of Blank Quality on Press-Formed PEKK/Carbon Composite Parts. *Materials* **2018**, *11*, No. 1063.
(28) Choupin, T.; Fayolle, B.; Régnier, G.; Paris, C.; Cinquin, J.; Brulé, B. A more reliable DSC-based methodology to study crystallization kinetics: Application to poly(ether ketone ketone) (PEKK) copolymers. *Polymer* **2018**, *155*, 109−115.
(29) Cortès, L. Q.; Caussé, N.; Dantras, E.; Lonjon, A.; Lacabanne, C. Morphology and dynamical mechanical properties of poly ether ketone ketone (PEKK) with meta phenyl links. *J. Appl. Polym. Sci.* **2016**, *133*, No. 43396.
(30) Choupin, T.; Debertrand, L.; Fayolle, B.; Régnier, G.; Paris, C.; Cinquin, J.; Brulé, B. Influence of thermal history on the mechanical properties ofpoly(ether ketone ketone) copolymers. *Polym. Cryst.* **2019**, No. e10086.
(31) Bertelo, C. A.; Garcia-Leiner, M. A.; Decarmine, A.; Defelice, S. F. Heat Treated Polymer Powders. U.S. Patent US2013/0323416 A12013.
(32) Decraemer, N.; Huze, D.; Ster, H.; Pascal, J.; Brulé, B. Method for the Thermal Treatment of Poly-Arylene Ether Ketone Ketone Powders Suitable for Laser Sintering. U.S. Patent US2018/0148572 A12018.
(33) Ruland, W. X-ray Determination of Crystallinity and Diffuse Disorder Scattering. *Acta Crystallogr.* **1961**, *14*, 1180−1185.
(34) Kepstan PEKK Resins for Extremely Demanding Applications, 2020. https://www.extrememateriels-arkema.com/en/product-families/kepstan-pekk-polymer-range.
(35) Kepstan 6002; Arkema: France, 2020. https://www.extrememateriels-arkema.com/en/materials-database/products/datasheet/Kepstan%C2%AE%206002.
(36) Foxtrot software can be obtained by sending a mail to foxtrot@xenocs.com. Software is free for non-profit usage, directly usable with Nexus and ESRF 2D data format.
(37) Wojdyr, M. Fityk: a general-purpose peak fitting program. *J. Appl. Crystallogr.* **2010**, *43*, 1126−1128.
(38) Mazzocchetti, L.; Scandola, M. Enzymatic Synthesis and Structural and Thermal Properties of Poly(ω-pentadecalactone-co-butylene-co-succinate). *Macromolecules* **2009**, *42*, 7811−7819.
(39) Mazzocchetti, L.; Scandola, M.; Jiang, Z. Random copolymerization with a large lactone enhances aliphatic polycarbonate crystallinity. *Eur. Polym. J.* **2012**, *48*, 1883−1891.
(40) dos Santos, F. A.; Iulianelli, G. C.; Tavares, M. I. Effect of microcrystalline and nanocrystals cellulose fillers in materials based on PLA matrix. *Polym. Test.* **2017**, *61*, 280−288.
(41) Bartczak, Z.; Vozniak, A. WAXS/SAXS study of plastic deformation instabilities and lamellae fragmentation in polyethylene. *Polymer* **2019**, *177*, 160−177.
(42) "XSACT: X-ray Scattering Analysis and Calculation Tool. SAXS & WAXS Data Analysis Software, 2020. http://www.xenocs.com/products/software.
(43) Vonk, C. G. Computerization of Ruland's X-ray Method for Determination of the Crystallinity in Polymers. *J.Appl. Crystallogr.* **1973**, *6*, 148−152.
(44) Balko, J.; Lohwasser, R. H.; Sommer, M.; Thelakkat, M.; Thurn-Albrecht, T. Determination of the Crystallinity of Semicrystalline Poly(3-hexylthiophene) by Means of Wide-Angle X-ray Scattering. *Macromolecules* **2013**, *46*, 9642−9651.
(45) Strobl, G. R.; Schneider, M. Direct evaluation of the electron density correlation function of partially crystalline polymers. *J. Polym. Sci., Polym. Phys. Ed.* **1980**, *18*, 1343−1359.
(46) Tencé-Girault, S.; Lebreton, S.; Bunau, O.; Dang, P.; Bargain, F. Simultaneous SAXS-WAXS Experiments on Semi-Crystalline Polymers: Example of PA11 and its Brill Transition. *Crystals* **2019**, *9*, No. 271.

(47) Krishnaswamy, R. K.; Kalika, D. S. Glass transition characteristics of poly(arylether ketone ketone) and its copolymers. *Polymer* **1996**, *37*, 1915−1923.
(48) Ruland, W. Crystallinity and Disorder Parameters in Nylon 6 and Nylon 7. *Polymer* **1964**, *5*, 89−102.
(49) Alexander, L. E. *X-ray Diffraction Methods in Polymer Science*; John Wiley & Sons, Inc: New York, 1969.
(50) Mo, Z.; Lee, K. B.; Moon, Y. B.; Kobayashi, M.; Heeger, A. J.; Wudl, F. X-ray Scattering from Polythiophene: Crystallinity and Crystallographic Structure. *Macromolecules* **1985**, *18*, 1972−1977.
(51) Rabiej, S. A comparison of two X-ray diffraction procedures for crystallinity determination. *Eur. Polym. J.* **1991**, *27*, 947−954.
(52) Blundell, D. J. On the interpretation of multiple melting peaks in poly(ether ether keton). *Polymer* **1987**, *28*, 2248−2251.
(53) Hsiao, B. S.; Gardner, K. H.; Cheng, S. Z. D. Crystallization of Poly(ary1 Ether Ketone Ketone) Copolymers Containing Terephthalate/lsophthalate Moieties. *J. Polym. Sci., Part B: Polym. Phys.* **1994**, *32*, 2585−2594.
(54) Choupin, T.; Fayolle, B.; Régnier, G.; Paris, C.; Cinquin, J.; Brulé, B. Isothermal crystallization kinetic modeling of poly(etherketoneketone) (PEKK) copolymer. *Polymer* **2017**, *111*, 73−82.
(55) Lee, Y.; Porter, R. S. Double-Melting Behavior of Poly(ether ether ketone). *Macromolecules* **1987**, *20*, 1336−1341.
(56) Ko, T. Y.; Woo, E. M. Changes and distribution of lamellae in the spherulites of poly(ether ether ketone) upon stepwise crystallization. *Polymer* **1996**, *37*, 1167−1175.
(57) Marand, H.; Alizadeh, A.; Farmer, R.; Desai, R.; Velikov, V. Influence of Structural and Topological Constraints on the Crystallization and Melting Behavior of Polymers. 2. Polly(arylene ether ether ketone). *Macromolecules* **2000**, *33*, 3392−3403.
(58) Velikov, V.; Marand, H. Studies of the enthalpy relaxation and the "multiple melting" behavior of semicrystalline poly(arylene ether ether ketone) (PEEK). *J. Therm. Anal.* **1997**, *49*, 375−383.
(59) Martinez, C. R.; Iverson, B. L. Rethinking the term "pi-stacking". *Chem. Sci.* **2012**, *3*, No. 2191.
(60) Hudson, S. D.; Davis, D. D.; Lovinger, A. J. Semicrystalline Morphology of Poly(aryl ether ether ketone)/Poly(ether imide) Blends. *Macromolecules* **1992**, *25*, 1759−1765.
(61) Okabe, Y.; Murakami, H.; Osaka, N.; Saito, H.; Inoue, T. Morphology development and exclusion of noncrystalline polymer during crystallization in PVDF/PMMA blends. *Polymer* **2010**, *51*, 1494−1500.
(62) Blundell, D. J.; Beckett, D. R.; Willcocks, P. H. Routine crystallinity measurements of polymers by d.s.c. *Polymer* **1981**, *22*, 704−707.
(63) Séguéla, R. Temperature dependance of the melting enthalpy of poly(ethylene terphthalate) and poly(aryl-ether-ether-ketone). *Polymer* **1993**, *34*, 1761−1764.
(64) Kong, Y.; Hay, J. N. The enthalpy of fusion and degree of crystallinity of polymers as measured by DSC. *Eur. Polym. J.* **2003**, *39*, 1721−1727.
(65) Li, C.; Strachan, A. Prediction of PEKK properties related to crystallization by molecular dynamics simulations with a united-atom model. *Polymer* **2019**, *174*, 25−32.
(66) Zoller, P.; Kehl, T. A.; Starkweather, H. W.; Jones, G. A. The Equation of State and Heat of Fusion of Poly(ether ether ketone). *J. Polym. Sci., Part B: Polym. Phys.* **1989**, *27*, 993−1007.
(67) Lee, Y.; Porter, R. S.; Lin, J. S. On the Double-Melting Behavior of Poly(ether ether ketone). *Macromolecules* **1989**, *22*, 1756−1760.
(68) Hoffman, J. D.; Davis, G. T.; Lauritzen, J. I. The Rate of Crystallization of Linear Polymers with Chain Folding. In *Treatise on Solid State Chemistry*; Hannay, N. B., Ed.; Springer: Boston, MA, 1976.
(69) Rault, J. The αc Transition in Semicrystalline Polymers: A New Look at Crystallization Deformation and Aging Process. *J. Macromol. Sci., Part C* **1997**, *37*, 335−387.
(70) Strobl, G. Colloquium: Laws controlling crystallization and melting in bulk. *Rev. Mod. Phys.* **2009**, *81*, 1287−1300.